International Journal of Pharmaceutics 378 (2009) 122–135

Contents lists available at ScienceDirect

International Journal of Pharmaceutics

journal homepage: www.elsevier.com/locate/ijpharm

Mapping of solution components, pH changes, protein stability and the elimination of protein precipitation during freeze–thawing of fibroblast growth factor 20

Haripada Maity*[1,3], Cyrus Karkaria, Juan Davagnino[2,3]

Biopharmaceutical Process Sciences, CuraGen Corporation, 322 East Main Street, Branford, CT 06405, USA

ARTICLE INFO

Article history:
Received 1 April 2009
Received in revised form 26 May 2009
Accepted 27 May 2009
Available online 6 June 2009

Keywords:
Fibroblast growth factor
Protein solubility
Protein stability
Folding/unfolding
Aggregation
Arginine
Salting out
Differential scanning calorimetry
Thermodynamics
Fluorescence
Circular dichroism

ABSTRACT

This study discusses the effect of key factors like containers, buffers and the freeze (controlled vs. flash freezing) and thawing processes on the stability of a therapeutic protein fibroblast growth factor 20 (FGF-20). The freezing profiles monitored by 15 temperature probes located at different regions in a 2-L bottle during freezing can be grouped into three categories. A rapid drop in temperature was observed at the bottom followed by the top and middle center of the bottle. The freeze–thawing behavior in a 50 ml tube is considerably uniform, as expected. Among phosphate, HEPES (4-(2-hydroxyethyl)-1-piperazine ethanesulfonic acid), citrate and histidine (each containing 0.5 M arginine-sulfate) buffer systems, a minimum pH change (0.4 pH unit vs. ~1.7 pH unit) was observed for the phosphate buffer system. Thawing in a 50 ml tube at room temperature standing resulted in a significant phase separation in citrate, histidine and HEPES buffers; however, phase separation was least in the phosphate buffer system. These phase separations were found to be temperature dependent. No effect of Polysorbate 80 on freeze–thawing of FGF-20 was observed. Significant concentration gradients in major buffer components and protein concentration were observed during freeze–thawing in a 2-L bottle. The segregation patterns of the various components were similar with the top and bottom layers containing lowest and highest concentrations, respectively. In the formulation buffer no pH gradient was formed, and the precipitation of FGF-20 during thawing at the top layer was related to an insufficient amount of arginine-sulfate and the precipitation at the bottom layer was due to a *salting out* effect. The precipitate generated during thawing goes into solution easily upon mixing whole solution of the bottle and the various gradient formations do not cause any irreversible change in structure, stability and isoform distribution of FGF-20. Comparison of slow freezing and flash freezing data suggests that the gradients in excipient and protein concentrations are mainly formed during thawing.

1. Introduction

Therapeutic proteins are generally frozen for short-term and long-term storage and undergo freezing course during the lyophilization process. The freeze–thawing method involves a variety of stresses that could be potentially damaging to the stability of proteins. The stresses associated with freeze–thawing methods are pH change, cold denaturation, effect of high solute concentrations on protein stability, and surface-induced denaturation at the ice–water interface (Chang et al., 1996; Wang, 2000; Arakawa et al., 2001). The extent of damage by these stresses depends on the conformational stability of proteins and the degree of irreversibility of the reaction caused by these stresses. Proteins with high thermodynamic stability and the ability to undergo reversible transition can overcome these stresses without any noticeable damage. So it is very important to investigate the biochemical and biophysical properties of therapeutic proteins with respect to freeze–thawing related stresses.

Heat transfer behavior primarily depends on temperature gradient, solution volume, container size and its architecture (Appendix A). pH changes and protein stability during freeze–thawing depends on buffer type. This study reports a detailed investigation of these factors and their effect on protein stability during

Abbreviations: FGF-20, fibroblast growth factor 20; BSA, bovine serum albumin; GdmCl, guanidinium chloride; CD, circular dichroism; HPLC, high performance liquid chromatography; HEPES, 4-(2-hydroxyethyl)-1-piperazine ethanesulfonic acid; TFA, trifluoroacetic acid; WCAS, West Coast Analytical Service, Inc.; NTU, Nephelometric Turbidity Unit.

* Corresponding author. Tel.: +1 215 498 3140.
E-mail address: haripada.maity@yahoo.com (H. Maity).
[1] Present address: ImClone Systems, A Wholly-Owned Subsidiary of Eli Lilly and Company, 59-61 ImClone Drive, Branchburg, NJ 08876, USA.
[2] Present address: KBI Biopharma, Biopharmaceutical Development, 1101 Hamlin Road, Durham, NC 27704, USA.
[3] Haripada Maity and Juan Davagnino were the previous employee of CuraGen Corporation.

0378-5173/$ – see front matter © 2009 Elsevier B.V. All rights reserved.
doi:10.1016/j.ijpharm.2009.05.063

freeze–thawing of a therapeutic protein fibroblast growth factor 20 (FGF-20). FGF-20 is an investigational therapeutic protein with a monomeric mass of 23 kDa and 211 amino acid residues, but in solution exists as a non-covalent dimer. The therapeutic potential of FGF-20 is to prevent oral mucositis, a common side effect of chemo- or radio-therapy by promoting both epithelial and mesenchymal cell proliferation (Jeffers et al., 2002; Alvarez et al., 2003). A link between FGF-20 and Parkinson's disease has also been reported (van der Walt et al., 2004; Wang et al., 2008). The primary structure of FGF-20 is known (Kirikoshi et al., 2000; Jeffers et al., 2001) and shows there are 2 free sulfhydryls located at C71 and C137. It has 1 tryptophan and 9 tyrosine residues that are especially useful for fluorescence measurements. FGF-20 has a high degree of sequence homology with FGF-9 (by 70%) and FGF-16 (by 64%). The structure of FGF-20 has not been published, but on the basis of the crystal structure of FGF-9 (Plotnikov et al., 2001), it can be anticipated that FGF-20 adopts a β-trefoil fold. Recently, structural characterization, solubility and stability of this molecule have been reported (Fan et al., 2007; Maity et al., in press).

This investigation highlights various key events during the freeze–thawing of FGF-20, which possesses complex solution properties. The primary objectives of this study are: (i) understanding temperature profiles in different containers, (ii) pH changes and protein stability in different buffer systems, (iii) surfactants- and surface-induced denaturation, (iv) mechanism of concentration gradient formation of major buffer components and protein, (v) concentration gradient and protein solubility, (vi) controlled freezing versus flash freezing and the (vii) biophysical characterization analysis using a variety of techniques. Results of these studies are critical for the development of a formulation and the freeze–thawing method.

2. Materials and methods

2.1. Materials

Purified FGF-20 was prepared by CuraGen Corporation, Branford, CT and the concentration was determined using the extinction coefficient of 0.97 ml mg^{-1} cm^{-1} at 280 nm. The observed absorbance at 280 nm was corrected for any contribution due to light scattering using the following equation and by measuring absorbance at 320 nm (Maity et al., in press):

$$A280_{correct} = A280_{obs} - 1.706 \times A320_{obs} \quad \text{(i)}$$

$A280_{obs}$ and $A320_{obs}$ are the observed absorbance values at 280 and 320 nm and $A280_{correct}$ is the corrected absorbance at 280 nm.

Guanidinium chloride (GdmCl) was purchased from M.P. Biomedicals, LLC. The concentration of GdmCl was determined from refractive index measurement using the following equations (Nozaki, 1972; Pace, 1986):

$$\text{For GdmCl,} \quad C = 57.147(\Delta N) + 38.68(\Delta N)^2 - 91.60(\Delta N)^3 \quad \text{(ii)}$$

here, C is the molar concentration and ΔN is the difference between the refractive index of the denaturant solution and the buffer solution at the sodium D line.

L-arginine was purchased from J.T. Baker and other chemicals were of molecular biology/analytical grades.

The composition of the formulation buffer is 50 mM sodium phosphate, 0.5 M arginine pH 7.0 and the pH was adjusted with sulfuric acid unless otherwise mentioned.

2.2. Methods

2.2.1. Monitoring temperature profile during freeze–thawing

Heat transfer profile was monitored in a 50 ml falcon tube and 2 L Teflon bottle containing 35 ml and 1.7 L of solution, respectively.

Fig. 1. Temperature sensor array in a 2-L Teflon bottle containing 1.7 L of a buffer composed of 20 mM histidine, 10% sucrose, and 0.02% (w/v) Polysorbate 20 at pH 6.0. Sensors were laid out to measure temperature at the walls on four sides, in the center, at the top, middle, and bottom of the bottle.

In the 2-L bottle, an array of 15 temperature sensors was placed (Fig. 1) to measure temperature changes during the freeze–thawing process. The sensors were laid at the walls on four sides, in the center, at the top, middle, and at the bottom of the bottle (Fig. 1). Care was taken during the construction that the array took up as little volume as possible, that the sensors were carefully mapped and placed in specific locations, and that there were little or no sharp edges or rough surfaces on the array that may alter freezing behavior. The 2-L bottle was filled with 1.7 L of buffer (10% sucrose, 20 mM histidine buffer, and 0.02% (w/v) Polysorbate 20 at pH 6.0.), then placed in the freezer at −80 °C, and allowed to freeze completely over the course of 48 h. Afterwards, the entire apparatus was taken out and allowed to thaw at room temperature for 48 h. In order to determine the effects of container size and volume on similar freeze–thawing processes, a 50 ml falcon tube containing 35 ml of solution was used as the smallest reasonable volume in which the sensor itself would not be too substantial a volume. Two tubes were fixed with one sensor in each. In one, the sensor was placed in the bottom, while in the other the sensor was suspended in the center of the liquid volume. These tubes were then placed in the same freezer and allowed to freeze completely, then thawed at room temperature. All the temperature profiles were monitored by TempTale 4 temperature probes manufactured by Sensitech.

2.2.2. Monitoring pH profile during freeze–thawing

pH changes during freezing were monitored by an InLab428 pH electrode (with FRISCOLYT-B fill solution, Model # 1920) made by Mettler Toledo. This electrode was connected to an Orion pH meter (Model # 920A+) and the electrode was capable of measuring pH in the temperature range of −30 to 80 °C.

Arginine at a concentration of 0.5 M was prepared in four different buffer systems with a concentration of 50 mM of either of the following: phosphate, histidine, citrate and HEPES. Polysorbate 80 was added at a concentration of 0.01% and the pH was adjusted to 7.0 with sulfuric acid and the final sulfuric acid concentration in the formulation buffer was about 0.23 M. Four 2-L bottles were filled with 1.6 L of each buffer. A temperature sensor and a pH electrode

were placed in the middle of the bottle. The bottles were frozen in a −20 °C freezer for about 40 h and then were transferred to room temperature, and allowed to thaw for 30 h.

To analyze the effect of various components of formulation buffer (50 mM sodium phosphate, 0.5 M L-arginine, 0.01% Polysorbate 80 pH 7.0), three 2-L bottles containing 1.6 L of 0.5 M arginine-sulfate (bottle-1), 50 mM sodium phosphate (dibasic and monobasic mix) (bottle-2) and formulation buffer (bottle-3) were frozen at −20 °C. Initial pH of all solutions was 7.0. Each bottle had a temperature sensor and a pH electrode in the middle section of the bottle. After approximately 40 h at −20 °C, the bottles were transferred to room temperature for thawing for a period of 30 h. The pH and temperature were measured for each bottle/buffer system and correction for the temperature compensation was made for the reported pH changes.

2.2.3. Mapping of component concentrations in protein and major formulation buffer components in a 2-L bottle during freeze–thawing

Two Teflon bottles (named as A and B) containing 1.6 L of 10 mg/ml FGF-20 solutions in formulation buffer were frozen at −80 °C and kept until used. These bottles were thawed at 4 °C (without shaking) until completely thawed which took about 60 h. Upon thawing, the bottles showed phase separation. Aliquots from different regions of the bottle (top, center, sides, and bottom) were sampled and another sample was collected after mixing whole solution of the bottle. These samples were analyzed to measure NTU, light scattering (LS), protein concentration, arginine concentration, pH, and aggregation by SEC–HPLC and isoform distribution by RP-HPLC. These samples were also sent to West Coast Analytical Service, Inc. (WCAS) for sulfate and phosphate analysis. Biophysical characterization was performed by measuring near-UV CD, fluorescence, denaturant induced unfolding, DSC, and second derivative UV spectroscopy.

2.2.4. Turbidity assessment by nephelometry

Nephelometric Turbidity Unit (NTU) was measured using undiluted sample in a Hach Ultra Model 2100AN turbidimeter with a small cell adaptor. NTU standards made by AMCO were used to check the variability of the instrument. A 3 ml sample was aliquoted into a 10 ml Pyrex glass tube and placed into the sample holder in order to measure the NTU value.

2.2.5. Turbidity assessment by light scattering (UV)

In order to assess turbidity, absorbance was measured at 340, 345, 350, 355 and 360 nm and then averaged. Absorbance was measured using a Shimadzu UV spectrophotometer (UV-2401) with a 1 cm path length cuvette.

2.2.6. Determination of arginine concentration by absorbance measurement

The concentration of arginine in the formulation buffer was determined by measuring the optical density at 240 nm using a UV spectrophotometer and Milli Q water was used as a blank. A set of standards was analyzed to produce a calibration curve. Samples containing protein were centrifuged using an Amicon Ultra-15 centrifuge filter unit to remove the protein from the buffer. The filtrate from each of these samples was analyzed. The calibration curve was used to assess the relative arginine concentration in the samples.

2.2.7. Determination of sulfate and phosphate concentrations

The sulfate and phosphate concentrations in different regions of the bottle were determined by West Coast Analytical Service, Inc. (WCAS). Ion exchange chromatography was used to determine both sulfate and phosphate concentrations.

2.2.8. Tertiary structure using near-UV CD spectra

Near-UV CD spectra were recorded using an AVIV 62DS instrument (AVIV Associates, Lakewood, NJ) with a cuvette having a 1 cm path length. The wavelength range used was 250–320 nm at a temperature of 20 °C. Data was recorded every 0.5 nm with an averaging time of 2 s and a band width of 3 nm. Each spectrum was an average of three scans. Protein samples (mixed (M), bottom center (BC), bottom side (BS), middle side (MS), middle center (MC) and perimeter precipitate (PP)) were collected from different regions of bottle-A (see Section 2.2.3). The collected samples were dialyzed in 50 mM phosphate (monobasic), 0.1 M sodium sulfate, at pH 7.0. Each sample was then diluted to a concentration of 0.39 mg/ml (monomer) using dialysis buffer and spectra were recorded. Protein in bottle-A contained 0.01% Polysorbate 80, and during dialysis, Polysorbate 80 will remain within the dialysis bag. There could be a heterogeneous distribution of Polysorbate 80 at different regions of the bottle. Therefore, the actual concentration of Polysorbate 80 is unknown. Assuming each sample contained 0.01% Polysorbate 80, the near-UV CD spectrum was recorded for the buffer containing 50 mM phosphate (monobasic), 0.1 M sodium sulfate, 0.01% Polysorbate 80, at pH 7.0. The buffer spectrum was then subtracted from that of the protein sample and the observed signal was converted to molar elipticity.

2.2.9. Fluorescence spectral analysis

Fluorescence spectra were recorded in the wavelength range of 300–400 nm using a PTI (Photon Technology International) fluorometer at two excitation wavelengths, 283 and 295 nm. Each data point was collected at an interval of 1 nm and both excitation and emission slits were set at 2 nm. Each spectrum represents a single scan. Protein samples at different regions of bottle-A were buffer exchanged in 50 mM phosphate, 0.5 M arginine, 0.01% Polysorbate 80, pH 7.0. Each sample was then diluted to a protein concentration (monomer) of 2.5 μM with 50 mM phosphate, 0.5 M arginine, 0.01% Polysorbate 80. The spectra were recorded at room temperature.

2.2.10. Second derivative near-UV absorption spectra

Second derivative near-UV absorption spectra were recorded using an Agilent 8453 UV–vis spectrophotometer in the wavelength range of 240–400 nm. Each data point was collected at an interval of 1 nm with an integration time of 0.5 s. Derivative order, filter length and polynomial degree were 2, 9, and 5, respectively. All samples from bottle-A and bottle-B (see Section 2.2.3) were dialyzed with respect to 50 mM phosphate, 0.1 M sodium sulfate, at pH 7.0. Dialyzed protein samples were diluted to 0.39 mg/ml (monomer) with the same dialysis buffer. Each spectrum is an average of five scans. All experiments were done at room temperature.

2.2.11. Thermal stability by differential scanning calorimetry (DSC)

Thermal unfolding of various freeze–thaw samples of FGF-20 was measured with a MicroCal VP-DSC at a protein concentration of 1 mg/ml in 50 mM phosphate, 0.5 M arginine 0.01% Polysorbate 80, pH 7.0. All samples were scanned in duplicate in the temperature range of 20–80 °C at a scan rate of 30 °C/h. The solutions were pressurized at about 60 psi in the capillaries during each scan. A buffer/buffer scan was subtracted from the buffer/protein scan and a range of the thermogram around the peak was selected. Baseline correction was then performed and the thermogram was normalized for protein concentration. The mid-point of thermal denaturation (T_m) was obtained from the peak maximum and calorimetric enthalpy (ΔH_{cal}) was calculated from the area under the heat capacity curve.

2.2.12. Measurement of stability by denaturant induced unfolding

Unfolding transitions were monitored by both circular dichroism (CD) and total fluorescence intensity using an AVIV 62DS instrument (AVIV Associates, Lakewood, NJ). This instrument is equipped with a right angle photomultiplier for fluorescence measurements, a thermoelectric cell holder, and a computer controlled syringe pump for titration. Both fluorescence and CD data were collected almost simultaneously. Fluorescence data was obtained with an excitation wavelength of 283 nm and emission was monitored using a 320 nm cut-off filter. Bandwidth and equilibration time were 3 nm and 10 min, respectively, and the signal averaging time was 15 s. The general procedure for the denaturant induced unfolding was followed as described by Eftink and Maity (2000). Change in the fluorescence signal was multi-phasic, so for simplicity, CD data was used for analysis using a two-state dimeric unfolding model involving native dimeric and unfolded monomeric forms (Maity et al., 2005).

Stability of three freeze–thaw samples from bottle-A, designated as "mixed", "perimeter precipitate," and "middle center," were measured for denaturant induced unfolding using guanidinium chloride (GdmCl). As a reference, stability of unfrozen FGF-20 (reference) solution was also measured. The sample and reference were buffer exchanged with respect to 50 mM phosphate, 0.5 M arginine, 0.01% Polysorbate 80, at pH 7.0. Due to the high absorbance of arginine at the far-UV region, unfolding experiments were performed in 0.1 M potassium phosphate (dibasic), 0.2 M potassium chloride and 9.9 mM arginine-sulfate, at pH 7.0 as a function of GdmCl concentration at 20 °C. Unfolding transitions were monitored by both CD and total fluorescence.

2.2.12.1. Data analysis. Two-state dimeric unfolding reactions can be written as

$$N_2 \Leftrightarrow 2U \tag{1}$$

here N_2 is the native dimer and U is the unfolded monomeric form. The equilibrium constant as a function of denaturant concentration can be written as

$$K_{un}(D) = \frac{[U]_e^2}{[N_2]_e} = \frac{2[P]_0 X_U^2}{(1 - X_U)} \tag{2}$$

here 'e' refers to the equilibrium condition and $[P]_0$ is the total subunit concentration. The mole fraction of unfolded monomer $X_U(D)$ can be written as (Maity et al., 2005)

$$X_U(D) = \frac{2K_{un}(D)}{K_{un}(D) + \sqrt{K_{un}^2(D) + 8K_{un}[P]_0}} \tag{3}$$

and the mole fraction of the native dimer will be

$$X_{N_2} = 1 - X_U(D) \tag{4}$$

The total subunit concentration $[P]_0$ can be expressed as

$$[P]_0 = 2[N_2]_e + [U]_e = 2[N_2]_e + \sqrt{K_{un}(D)[N_2]_e} \tag{5}$$

To determine thermodynamic parameters of unfolding reactions, the signal should be related to the mole fraction of molecules in a given macrostate i by the following equation (Eftink and Maity, 2000; Eftink, 1994):

$$S = \sum_{i=1}^{n} X_i S_i \tag{6}$$

here, X_i and S_i are the mole fraction and intrinsic relative signal of state i, respectively. The analysis assumed a linear free energy relationship to describe the unfolding reaction and it can be expressed as

$$\Delta G_{un}^0(D) = \Delta G_{0,un}^0 - m[D] \tag{7}$$

$\Delta G_{0,un}^0$ is the unfolding free energy in the absence of denaturant, $m = -d\Delta G_{un}^0(D)/d[D]$ and it is directly correlated with the change in accessible surface area upon unfolding (Myers et al., 1995), $[D]$ is the denaturant concentration and

$$\Delta G_{un}^0(D) = -RT \ln K_{un}(D) \tag{8}$$

It is important to note that CD and fluorescence intensity of native and unfolded states may depend on perturbing condition, so there could be non-zero baseline slopes and it can be expressed as

$$S_i(D) = S_{i,0} + s_{l,i}[D] \tag{9}$$

$s_{l,i} = dS_i/d[D]$ is the baseline slope, S_i refers to any signal for a given macrostate and $S_{i,0}$ is the signal in the absence of denaturant. The entire transition data, including terms for baseline regions, was analyzed by a non-linear least-squares program including Eqs. (1)–(9) using SigmaPlot 8.0.

2.2.13. Reverse phase high performance liquid chromatography (RP-HPLC)

RP-HPLC experiments were performed with an Agilent 1100 HPLC system using a SUPELCO Discovery® BIO Wide Pore C5 (a covalently bonded pentylsilane) HPLC column along with a Discovery® BIO Wide Pore C5 guard column containing spherical silica with a 300 Å pore diameter. Various freeze–thaw samples were buffer exchanged with formulation buffer without Polysorbate 80 and at the end of buffer exchange, 0.01% Polysorbate 80 was added. Using formulation buffer, all freeze–thaw samples were diluted to 0.5 mg/ml. The column was operated with a flow rate of 0.6 ml/min and the column thermostat was set at 55 °C. Mobile phase-A and -B were 40% and 80% acetonitrile, respectively with 0.1% trifluoroacetic acid (TFA). Chromatograms were obtained by monitoring absorbance at 214 nm.

2.2.14. Size exclusion chromatography–High performance liquid chromatography (SEC–HPLC)

SEC–HPLC experiments were performed with Agilent 1100 HPLC system using a size exclusion HPLC column (Bio-Sil SEC-250, 0.78 cm × 30 cm, Bio-Rad) and the composition of the mobile phase was 100 mM sodium phosphate, 1 M arginine-HCl, pH 7.0. The column was operated with a flow rate of 0.4 ml/min and the column temperature was set at 20 °C. Chromatograms were obtained by monitoring absorbance at 280 nm.

3. Results and discussion

3.1. Temperature profile during freeze–thawing

Heat transfer will depend on the temperature difference, volume of the solution, surface area of the container, size, contours of vial design, thickness, and the thermal conductivity of the means through which heat transfer occurs (see Appendix A).

Data obtained from the temperature sensors in the 2-L bottle shows that it took about 12 h to reach a stable temperature of about −80 °C throughout the bottle. As shown in Fig. 2A, all traces can be grouped reasonably into three categories of behavior. The traces shown in shades of blue are sensors at the bottom of the bottle; traces in orange are in the middle level of the bottle; traces in green are at the top of the bottle. In the legend, the location of the probes is given by compass directions, where N is north, E is east, W is west, S is south, and C is center. This direction is paired with the letter to define the level in the bottle; B for bottom, M for middle, and T for top. All sensors were vertically aligned with the other sensor on the same cardinal direction, and horizontally aligned on the same plane as the other sensors of the same level. Fig. 2A can be simplified to a single trace representative for each of the three regional behaviors,

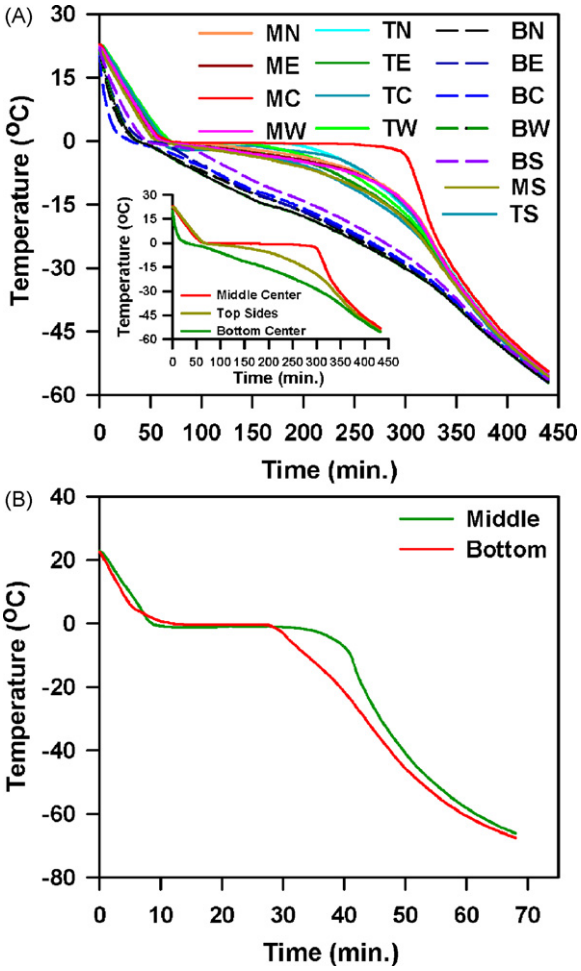

Fig. 2. (A) Temperature profiles during freezing in different regions of the bottle (see legend of Fig. 1) obtained from all 15 TempTale temperature probes. In the legend the location of the probes are given by compass directions, where N is north, E is east, W is west, S is south, and C is center. This direction is paired with the letter to define the level in the bottle, B for bottom, M for middle, and T for top. *Insert*: Temperature profiles during freezing obtained from three select probes with matching color regions of the bottle mentioned in Fig. 1. This figure is obtained from (A). (B) Temperature profiles during freezing in the middle and bottom region of a 50 ml falcon tube containing 35 ml of a buffer composed of 20 mM histidine, 10% sucrose, and 0.02% (w/v) Polysorbate 20 at pH 6.0.

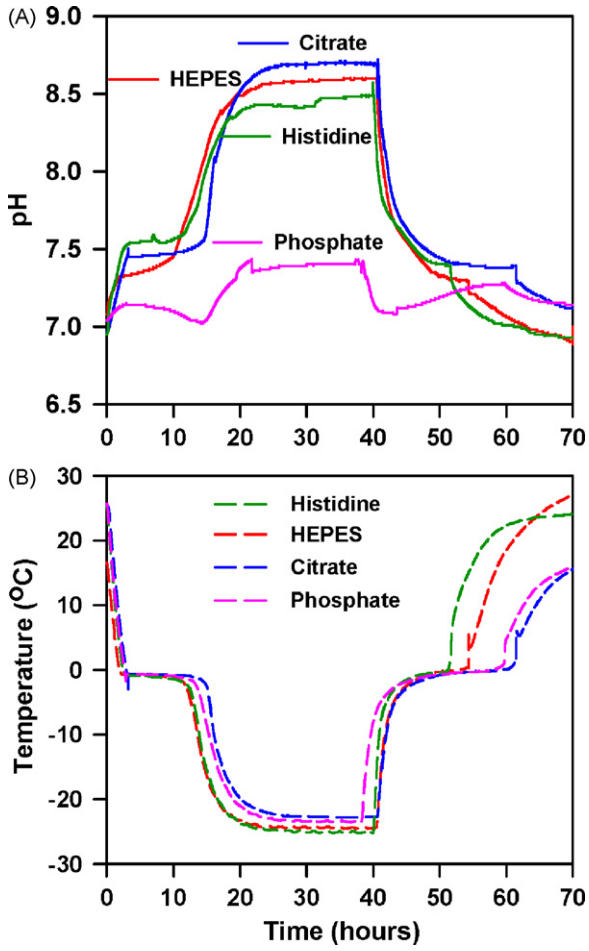

Fig. 3. pH (A) and temperature (B) profiles of various buffers during freeze–thawing in 2-L Teflon bottles each containing 1.6 L of solution. The temperature and pH probes were placed in the middle center of the bottle. The four buffer systems were 50 mM of histidine, citrate, phosphate and HEPES and each contain 0.5 M of arginine pH 7.0. pH of these buffers was adjusted by sulfuric acid.

which is displayed in the *insert* of Fig. 2A (see also Fig. 1). Here the behaviors indicate the nature of the freezing process in different parts of the bottle.

At the bottom of the bottle, temperature drops rapidly during the initial phases of chilling and continues to chill after passing the freezing point. This temperature profile suggests that chilling is most rapid at the bottom of the bottle and ice formation is the fastest. The chilling is still the most intense at the bottom and the ice is chilling as it is formed even before the water above is frozen. The second region of interest is in the middle center of the bottle. At this location the liquid cools much slower than the bottom and upon reaching the freezing point it holds steady at that temperature for a prolonged period. So the ice formation in this region is very slow and steady. The other freezing profile describing the behavior of the top and sides is the trace that falls between these two. This behavior shows the same temperature dropping behavior after hitting the freezing point as the bottom sensors, but it is not as severe. This trend suggests that the top and sides are losing energy faster than the material more interior to the bottle, but the bottom of the bottle shows the most rapid heat transfer.

Regional freeze–thawing behavior in a small vial is expected to be minimum, i.e., considerably uniform traces are anticipated throughout the vial. Fig. 2B shows the temperature profiles compared between the middle and the bottom of the 50 ml falcon tube. Here total freezing to the same temperature point as cited in the large bottle took only 2 h instead of 12 h. From the graph it is clear that while there is a slight divergence between the middle probe and bottom probe of about 15 min, during the ice formation period, the freezing behavior in the 50 ml vial is more consistent throughout. So it is reasonable to assume that the freezing behavior should be consistent throughout the 5–10 ml small vials. The thawing profiles are apparently mirror images to the freezing profiles (not shown). The temperature profiles of the thawing process in the 2 L bottle are shown in Figs. 3B and 4 and these also demonstrate that the temperature profiles of the freezing and thawing process are apparently mirror images of each other.

3.2. *pH profile during freeze–thawing*

pH changes during freeze–thawing can have a significant effect on the stability of proteins. It is well known that the pH of sodium phosphate buffer decreases by about 3 pH units upon freezing due to the crystallization of disodium salt (Gómez and Pikal, 2001; Pikal-Cleland et al., 2002; Anchordoquy and Carpenter, 1996). So it is very important to know the pH profiles during freeze–thawing of the potential buffers that could potentially be used for formulation.

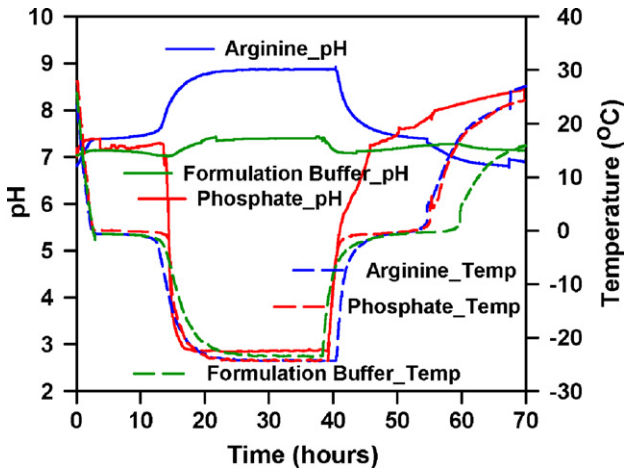

Fig. 4. pH and temperature profiles during freeze–thawing of formulation buffer and its components. These experiments were done in a 2-L bottle containing 1.6 L of solution. See Section 2.2.2 for detail.

Fig. 3 shows the temperature and pH profiles of four different buffer systems. With the exception of the phosphate buffer, all the other buffer systems showed a significant increase in pH, from an initial pH of 7.0 to 8.4–8.7. Interestingly, the formulation buffer showed an increase of only 0.4 pH units. In order to understand this observation, the individual components of the formulation buffer (arginine and phosphate) were subjected for freeze–thawing separately. Fig. 4 shows that the pH of the 0.5 M arginine-sulfate solution increases from 7.0 to 8.8. On the other hand, the pH of the phosphate solution decreases to 3.0. The pH changes of arginine and phosphate solutions are in opposite directions, resulting in the small pH changes. The opposite pH shift of the arginine and phosphate components explains the stability of the pH of the formulation buffer upon freezing. It can be concluded that the phosphate-arginine formulation gives an excellent pH stability during freeze–thawing in comparison to the other buffer systems studied here. The considerable increase in pH of citrate, histidine and HEPES buffers (Fig. 3A) is probably due to the predominant pH increment effect of arginine-sulfate.

3.3. *Effect of different buffer systems on the freeze–thaw behavior of FGF-20*

In order to understand the effect of four different buffer systems on the freeze–thaw behavior of FGF-20, freeze–thaw studies were performed in a 50 ml falcon tube containing 25 ml solution with a protein concentration of 10 mg/ml. Four different buffer systems used were phosphate, citrate, histidine and HEPES all at a concentration of 50 mM. Each buffer system contains 0.5 M of L-arginine and 0.01% Polysorbate 80, and pH was adjusted to 7.0 with sulfuric acid. Tubes were frozen at −20 °C overnight and each tube was then thawed at four different conditions: (i) room temperature standing, (ii) room temperature shaking, (iii) 4 °C standing, and (iv) 4 °C shaking. As discussed under Section 3.1, the temperature profile during freeze–thawing would be almost uniform throughout the solution for the 50 ml falcon tube containing 25 ml solution.

Fig. S1 (supplementary figure) shows the tubes with four different buffer systems thawed at room temperature standing. A small amount of precipitate at the bottom and a significant amount of material floating out of solution in the top portion of these tubes was present with HEPES, histidine and citrate buffer systems, but not so much in the phosphate buffer system. Samples were collected from the cloudy top and clear middle layers of tubes by carefully pipetting out. The amount of bottom layer precipitate was not enough for collection and subsequent analysis. Interestingly, when the cloudy top layers were kept in an ice bath, the solutions became clear. These clear solutions became cloudy at room temperature within about an hour and again became clear when kept in an ice bath. This reversible change in visual appearance of the top layer can be represented as

$$\text{Cloudy top layer (at room temperature)} \rightleftarrows \text{clear top layer (in ice bath)}$$

When the bottom precipitate, turbid Top and clear Middle layers were mixed, a clear solution was obtained.

However, after the cloudy top layers became clear in the ice bath, the samples were left in 4 °C in the fridge overnight. After about 10 h it was observed that all the top layers remained clear except for the citrate buffer system. At this stage, when all the top layers were kept in room temperature for 1 h, all samples became cloudy and upon putting these samples back in the ice bath, only solutions in phosphate and HEPES buffer systems became clear, whereas the solutions in citrate and histidine buffer systems remained cloudy. Table 1 shows systematic visual observation for the temperature effects on the cloudy top layers in different buffer systems obtained after thawing at room temperature standing. These data shows that phosphate and HEPES buffer systems are better for FGF-20 in comparison to citrate and histidine. The formulation buffer contains phosphate and detailed characterization of FGF-20 in different layers has been done in the formulation buffer only (Section 3.3.1).

Thawing with shaking either at 4 °C or room temperature (RT) did not generate a gradient in solute and protein concentration, and consequently no noticeable phase separation was observed. The tubes that were thawed at 4 °C with standing also did not show any turbidity (in comparison to thawing at room temperature standing) in the top layer because solubility of FGF-20 is higher at low temperature (see Section 3.3.1; Maity et al., in press).

As mentioned above, after thawing, top layers were more cloudy in HEPES, histidine and citrate buffer systems than in phosphate buffer. This is probably due to the difference in pH change during freezing (Fig. 3) as well as from a buffer effect. However, the

Table 1
Step-wise visual observation of temperature dependent changes in the physical appearance of FGF-20 solutions in the different layers of four buffer systems. The composition of various buffers was 50 mM X (X = phosphate, citrate, HEPES, and histidine), 0.5 M L-arginine, 0.01% Polysorbate 80 pH 7.0. pH was adjusted with sulfuric acid.

Buffer system	Section of the tube	1. Right after thawing and pooling (RT)	2. When in ice bath right after pooling	3. After fridge overnight	4. After out for 1 h (RT)	5. Back in ice bath
Phosphate	Top	**Cloudy**	Clear	Clear	**Cloudy**	Clear
Phosphate	Middle	Clear	Clear	Clear	Clear	Clear
Citrate	Top	**Cloudy**	Clear	**Cloudy**	**Cloudy**	**Cloudy**
Citrate	Middle	Clear	Clear	Clear	Clear	Clear
HEPES	Top	**Cloudy**	Clear	Clear	**Cloudy**	Clear
HEPES	Middle	Clear	Clear	Clear	Clear	**Clear**
Histidine	Top	**Cloudy**	Clear	Clear	**Cloudy**	**Cloudy**
Histidine	Middle	Clear	Clear	Clear	Clear	Clear

Table 2
Various parameters of freeze–thaw samples (50 ml falcon tubes) of FGF-20.

Sample ID	pH	Protein concentration (mg/ml)	Osmolality (mOsm/kg)	Turbidity[a] (340–360 nm)	NTU
Top	7.01	5.05	294	0.086	13.3
Middle	6.92	11.06	674	0.052	4.57
All mixed	6.91	10.26	529	0.035	8.28

[a] Average of absorbance measured at 340, 345, 350, 355 and 360 nm.

cloudiness in the top layer in all the buffer systems is primarily related to the lower arginine-sulfate concentration in comparison to clear middle layer (Sections 3.5.1 and 3.5.2). Though the temperature profiles of freeze–thawing in a 50 ml falcon tube would be more uniform (Fig. 2B) than in a 2 L bottle, the concentration gradient of various components mainly occurs during thawing (Section 3.5.2).

3.3.1. Characterization of protein at different layers obtained after thawing at room temperature standing in phosphate buffer system in a 50 ml tube

Thawing at 4 °C with or without shaking did not produce observable turbidity, so the samples were collected from the top and middle layers of tubes thawed at room temperature standing. The amount of bottom layer precipitate was insignificant for subsequent analysis. Top, middle and all mixed (top + middle + bottom) freeze–thaw samples were analyzed for pH, osmolality, protein concentration and turbidity (by nephelometry and light scattering). These samples were also analyzed by RP-HPLC for isoform distribution and the conformational stability was measured by DSC and guanidinium chloride induced unfolding. Concentration of buffer components at different layers will be different, so top, middle and all mixed samples were dialyzed in 50 mM phosphate, 0.5 M arginine-sulfate, 0.02% Polysorbate 80 at pH 7.0 for analysis. As Polysorbate 80 will not be dialyzed (even though the dialysis buffer contains Polysorbate 80) due to its large size, we would assume there is no significant gradient in the Polysorbate 80 concentration across the different layers.

Table 2 lists pH, protein concentration, osmolality and turbidity (by nephelometry and light scattering) in the phosphate buffer system. pH values of all the samples were very similar and at around pH 7. Consistent with the visual appearance of turbidity, data from light scattering and nephelometry was higher for the top layer. Both protein concentration and osmolality of the top layer were lower than the middle layer, and they were related to each other, i.e., the higher the protein concentration the higher the osmolality. We also observed that arginine concentration in the top layer was lower than the middle layer that causes lower osmolality in the top layer. Appearance of turbidity at the top layer for thawing at room temperature standing is related to the lower solubility of FGF-20 as the arginine-sulfate concentration was lower (Maity et al., in press) in this layer. Solubility of FGF-20 is higher at lower temperature (Maity et al., in press), so the turbid top layer became clear when incubated in an ice bath and became turbid at room temperature and this interchange was found to be reversible. Solubility of FGF-20 increases with increasing arginine concentration, at least up to 0.5 M arginine, and a *salting out* effect was observed at higher (1.5 M) arginine concentration (Maity et al., in press). In addition, solubility of FGF-20 is higher at 4 °C than at room temperature in the phosphate buffer system (Maity et al., in press).

Table 3
Thermal stability parameters determined from DSC profiles of freeze–thaw samples of FGF-20 (50 ml falcon tubes) as well as mid-point of transitions obtained from GdmCl induced unfolding.

Sample ID	T_m (°C)	ΔH_{cal} (kcal/mol)	C_m (M) (unfolding by GdmCl)
Top layer	58.6	105.4	1.74
Middle layer	58.5	101.1	1.75
All mixed	58.4	100.1	1.75
Reference	59.0	102.0	1.75

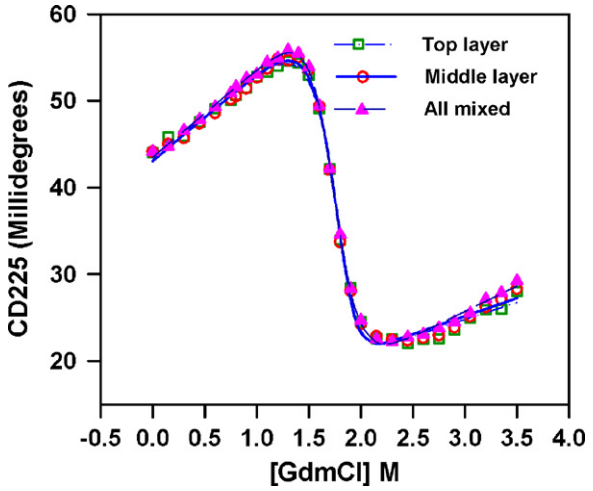

Fig. 5. GdmCl induced unfolding of FGF-20. Top layer, middle layer and all mixed samples were obtained from the freeze–thaw experiments that were done in 50 ml falcon tubes containing 10 mg/ml of FGF-20 in formulation buffer. Thawing was done at room temperature with standing. Initial buffer composition for the unfolding experiment was 0.1 M potassium phosphate (dibasic), 0.2 M KCl, 19.1 mM arginine (sulfate) pH 7.0. Titration was done by 5.28 M GdmCl solution containing 0.1 M potassium phosphate (dibasic), 0.2 M KCl, 10 mM arginine (sulfate) pH 7.0. Protein concentration was 8.3 μM (monomer). Unfolding transitions were monitored by far-UV CD at 225 nm at 20 °C.

Table 3 shows that both thermal transition temperature (T_m) and calorimetric enthalpy were very similar among all the samples. Fig. 5 shows GdmCl induced unfolding of FGF-20 in the top and middle layers as well as mixed freeze–thaw samples, monitored by far-UV CD at 225 nm. The unfolding transition curves for all the samples were almost super-imposable to each other, and similar behavior was found for the fluorescence signal. Table 3 also shows that mid-points of GdmCl induced unfolding transitions of all the samples were similar. Both DSC data and GdmCl induced unfolding transitions suggest that there was no change in stability among various samples. RP-HPLC data shows no noticeable difference in the isoform distribution among all the samples (not shown). It is very important to note that heterogeneous distribution of solutes and protein concentration did not cause any detectable irreversible change in the stability of FGF-20.

3.4. Effect of Polysorbate 80 on the precipitation of FGF-20 during thawing in a 50 ml tube

Surfactants have been reported to be useful in preventing surface-induced denaturation of protein during freezing (Chang et al., 1996). The effect of Polysorbate 80 on the opalescence of the FGF-20 solution during thawing was tested at Polysorbate 80 concentrations of 0.005, 0.010, 0.025, 0.050, and 0.1% (w/v) in the formulation buffer with 10 mg/ml protein. These samples were subjected to freezing for 24 h in a −80 °C freezer and thawed at two different conditions: room temperature standing and 4 °C standing.

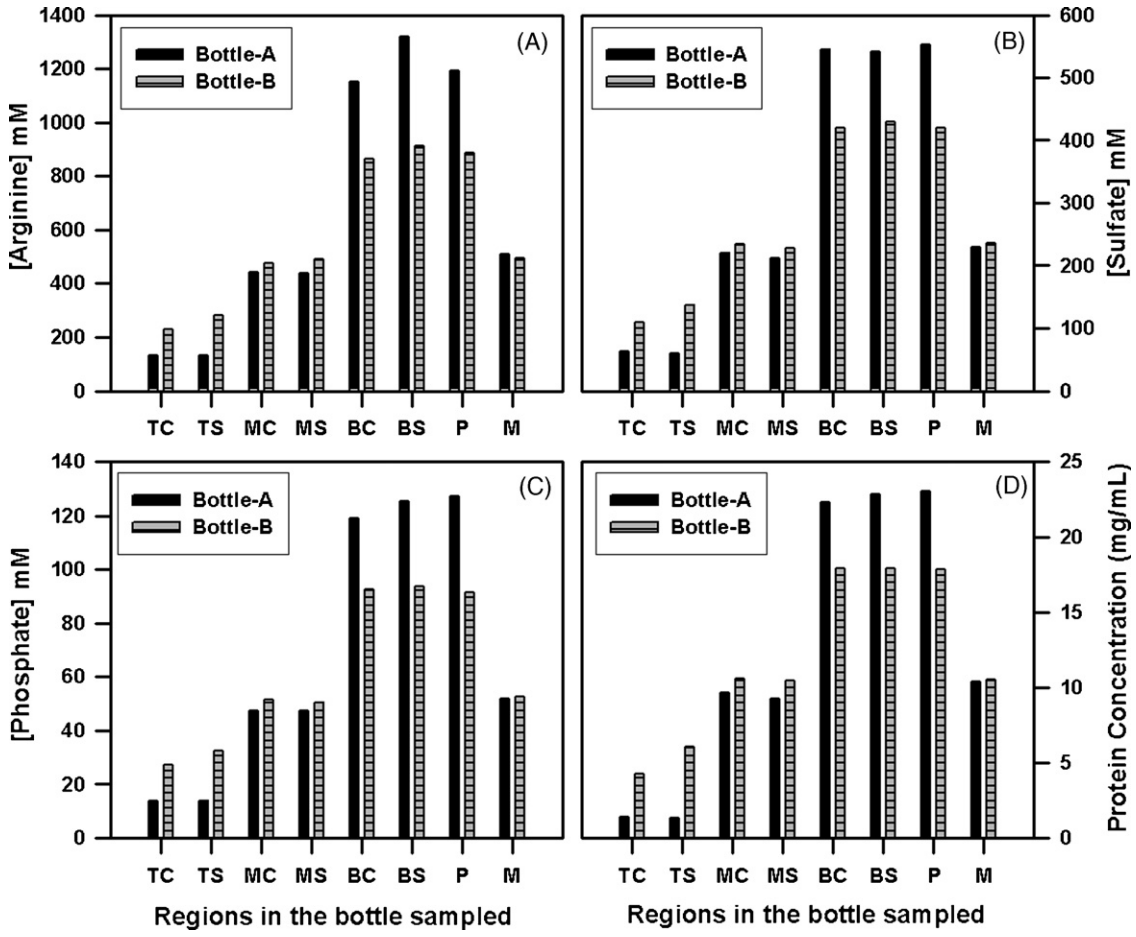

Fig. 6. Concentration of arginine (A), sulfate (B), phosphate (C) and protein (D) in samples collected from different regions in the 2-L bottles A and B after thawing in a cold room at 4 °C without shaking. TC, TS, MC, MS, BC, and BS refer to top center, top side, middle center, middle side, bottom center and bottom side regions of the bottle, respectively, P refers to the precipitate obtained at the bottom, and M refers to the mixed sample obtained after gentle shaking of the bottle at the end of complete thawing.

The samples were analyzed for protein concentration and turbidity by light scattering. All tubes thawed at RT showed opalescence with no significant difference in pattern with respect to protein concentration and turbidity including the tube that contained no Polysorbate 80. On the other hand, all the tubes thawed at 4 °C were clear. These results indicate that the thawing method, not the concentration of Polysorbate 80, has an effect on the presence or absence of opalescence in FGF-20 solution during thawing at room temperature standing.

3.5. *Freeze–thaw studies in a 2-L bottle*

Freeze–thaw studies in 50 ml tubes have provided important information about the nature of the precipitation problem. As heat transfer depends on the size and type of container in addition to other factors (see Section 3.1; Appendix A), freeze–thaw studies were performed in a 2-L Teflon bottle containing 1.6 L of solution. Freezing was done at −80 °C (except the flash freezing that was done in liquid nitrogen) and thawing was performed at 4 °C unless otherwise mentioned. These experiments were performed to understand the mechanism of gradient formation of various components of protein solution during freeze–thawing as well as to find the method to thaw the frozen bottle without protein precipitation.

3.5.1. *Mapping of component concentrations in protein and major formulation buffer components in a 2-L bottle*

Upon thawing, the top layers of both the bottles (A and B) (see Section 2.2.3) were turbid whereas only bottle-A had precipitate at the bottom (Fig. S2, supplementary figure). This difference is probably due to the difference in location of the bottles in the freezer during freezing. These two bottles were frozen in a −80 °C freezer along with many other bottles and the freezing behavior may be different to some extent at different locations. However, turbidity (by nephelometry and LS) of the solutions from different regions of the bottle varied significantly. Very high NTU and LS values in the top layer were observed, supporting the visual observation. Bottom layer samples also showed high turbidity compared to the side and center samples. The sample taken after mixing these layers of solution had NTU and LS readings similar to that of center or side samples. Bottle-A showed a higher degree of turbidity at top side, top center, middle center, bottom side, bottom center and bottom perimeter than bottle-B. However, the NTU and light scattering values obtained after thoroughly mixing the bottles were low and similar.

The results of the arginine distribution are shown in Fig. 6A. A more pronounced arginine gradient is measured in bottle-A than in bottle-B. While the minimum and maximum arginine concentrations for bottle-A were 132 mM (top) and 1320 mM (bottom), respectively, the corresponding values for bottle-B were 230 and 911 mM. The sulfate and phosphate concentrations in these samples were measured by ion exchange chromatography by West Coast Analytical Service Inc., and the results are provided in Fig. 6B and C, respectively. The results show a gradient very similar to that found for arginine, with the top being low and the bottom showing high levels of sulfate and phosphate. Bottle-A results also show greater limits when compared to bottle-B. As expected, a similar pattern

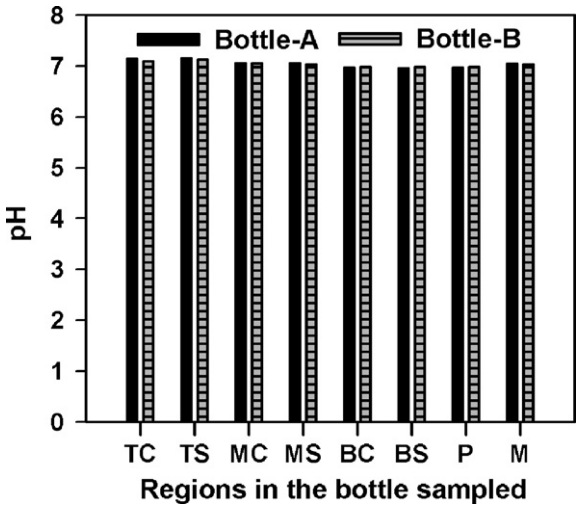

Fig. 7. pH of samples collected from different regions in the 2-L bottles A and B after thawing in a cold room at 2–8 °C without shaking. TC, TS, MC, MS, BC, BS, P, and M have the same meaning as explained in the caption of Fig. 6.

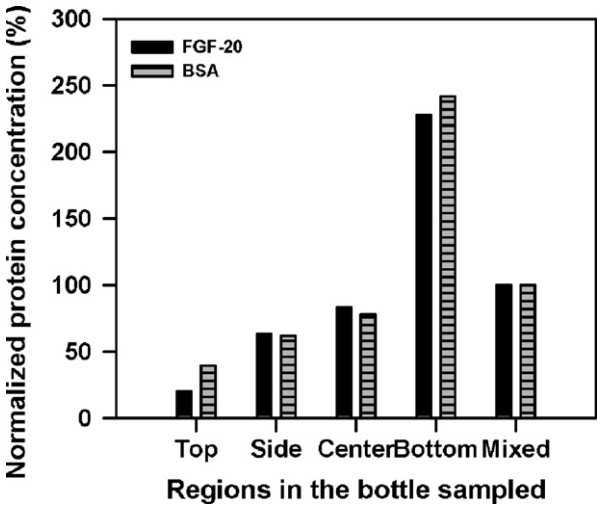

Fig. 8. Concentration of FGF-20 and BSA in samples obtained from different regions in 2-L bottles after thawing in a cold room at 4 °C without shaking. The concentrations of FGF-20 and BSA were 10 mg/ml and 4.9 mg/ml, respectively and these concentrations have been normalized.

of the concentration of FGF-20 distribution was observed. Fig. 6D shows the FGF-20 concentration at different locations in the two bottles. The top turbid layer has the lowest concentration of protein and the bottom layer has the highest concentration. Bottle-A showed a steeper protein gradient compared to bottle-B. pH of all the samples remained very similar being ~7.1 and ~7.0 at the top and bottom layer, respectively (Fig. 7). SEC–HPLC data shows that soluble FGF-20 does not form aggregates in any of the fractions obtained from different regions of the bottles (not shown).

As mentioned above, solubility of FGF-20 strongly depends on arginine and increases with increasing arginine concentration (at least up to 0.5 M arginine) and a *salting out* effect was observed at higher (1.5 M) arginine concentration (Maity et al., in press). Among chloride, sulfate and phosphate salts of arginine, solubility is maximum in arginine-sulfate. For example, solubility values of FGF-20 at 0.2 M, 0.5 M and 1.5 M arginine-sulfate in 50 mM phosphate pH 7.0 are 1.7 mg/ml, >40 mg/ml and 15 mg/ml, respectively (Maity et al., in press). In bottle-A, solution in the top was cloudier than bottle-B. This is because both the arginine and sulfate concentrations were lower in bottle-A than bottle-B (Fig. 6A and B). Differences in arginine and sulfate also explains the difference in protein concentration in the top layer of the two bottles. At the middle section of these bottles, arginine and sulfate concentrations were about 0.5 M and 220 mM, respectively, and solubility of FGF-20 in this condition is about 40 mg/ml and that is why the middle section of the bottles was clear. Protein precipitation was observed after thawing at the bottom of bottle-A, not for bottle-B and this is due to the *salting out* effect. Arginine, sulfate and protein concentrations at the bottom of the bottle-A were higher than in bottle-B that causes *salting out* effect in the bottle-A. The arginine-sulfate concentration in bottle-B was not high enough to produce the *salting out* of the protein and therefore FGF-20 did not precipitate. The reversibility in the structure and stability of the protein in the precipitated form as well as from the different regions of the bottles after thawing, was tested by biophysical characterization, SEC–HPLC and RP-HPLC.

In order to evaluate whether the segregation pattern of protein concentration observed for FGF-20 is common to other proteins, freeze–thaw studies were performed with 4.9 mg/ml of BSA in the same formulation buffer in exactly the same way with the same size Teflon bottle as performed for FGF-20. Fig. 8 shows that protein concentration distribution after freeze–thawing is very similar. Although the same segregation pattern was observed for BSA and FGF-20, high turbidity values and visible opalescence were detected only in the FGF-20 solution. We conclude that the two proteins segregate in a similar way to different regions of the bottle during the freeze–thawing process. However, turbidity or opalescence was detected only in the FGF-20 solution probably due to lower solubility of this protein.

3.5.2. Mechanism of gradient formation of component concentrations in protein and major formulation buffer components in a 2-L bottle

In an effort to understand the basis of the formation of the concentration gradient for excipients and active found in all the 2-L bottles, the composition of the floating ice in the bottle was analyzed. One bottle containing 1.6 L of 4.9 mg/ml BSA solution in formulation buffer and another bottle with 1.6 L of formulation buffer were frozen at −80 °C. These bottles were thawed for 30 h at 4 °C, then the bottle was cut above the fluid line and the remaining ice (about 250 g) floating on the top of each solution was removed and placed in a separate container and allowed to thaw completely at 4 °C. The arginine and protein concentrations were measured in the fluid obtained after the first 30 h of thawing as well as in the remaining melted ice solution. In the bottle containing formulation buffer, the ice had an arginine concentration of 94 mM, while the remaining solution had an arginine concentration of 586 mM. In the bottle containing BSA solution, the ice had an arginine concentration of 134 mM and the remaining solution had an arginine concentration of 871 mM. The concentration of BSA distribution showed a very similar segregation to that of the arginine (very low in the ice, 1 mg/ml, and high in the remaining solution, >7 mg/ml) mimicking what we have seen throughout the study where components migrate together during the freeze–thaw cycle. We conclude from this experiment that as the solutions are thawing, the salts and proteins melt out of the ice and leave ice that contains mostly water at the top of the solution. This process dilutes the top solution and concentrates the bottom solution.

To separate the freezing from the thawing effect on the excipient and protein gradient, two 2-L Teflon bottles containing 1.6 L of 10 mg/ml of FGF-20 in formulation buffer were flash frozen by submerging in liquid nitrogen for approximately 20 min until the bottle appeared completely frozen. These bottles were then transferred to a −80 °C freezer until used. One bottle was taken out of the freezer and pieces of ice were sampled from different regions of the frozen bottle, then thawed at 4 °C and analyzed for arginine and protein concentration. Another bottle was thawed completely

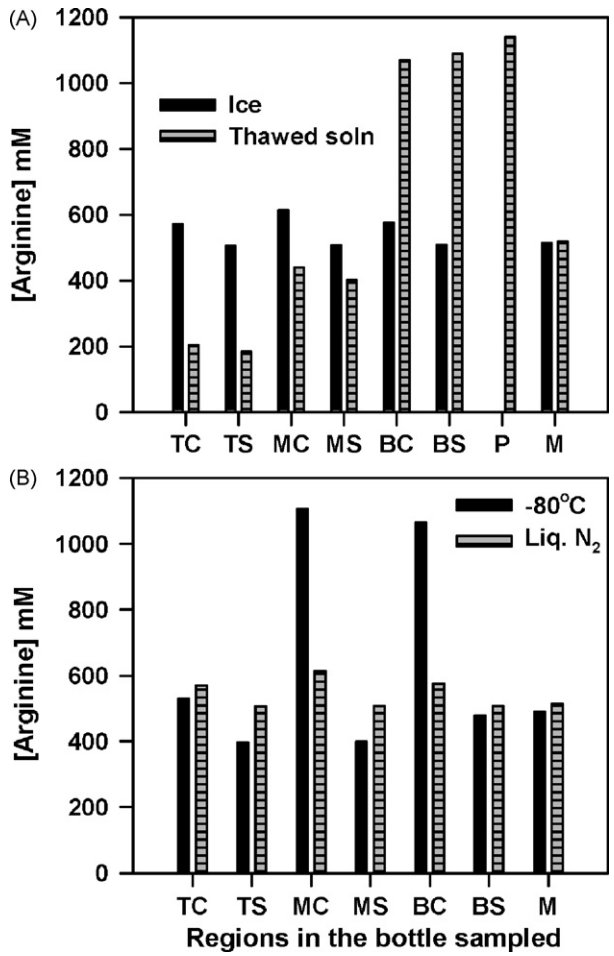

Fig. 9. (A) Concentrations of arginine in different regions of 2-L bottles containing 1.6 L of 10 mg/ml FGF-20 in formulation buffer. These bottles were flash frozen in liquid nitrogen. One bottle was thawed in cold room at 4 °C and then samples were collected from different regions. For the other bottle, frozen samples were collected from different regions, then thawed at 4 °C and analyzed. TC, TS, MC, MS, BC, BS, P, and M have the same meaning as explained in the caption of Fig. 6. (B) Concentrations of arginine in different regions of 2-L bottles containing 1.6 L of 10 mg/ml FGF-20 in formulation buffer. One of these bottles was flash frozen in liquid nitrogen and the other one was frozen at −80 °C. Frozen samples were collected from different regions of these bottles and then thawed at 4 °C and analyzed. TC, TS, MC, MS, BC, BS, P, and M have the same meaning as explained in the caption of Fig. 6.

at 4 °C, then samples from different regions were collected and also analyzed for arginine and protein concentration. Fig. 9A shows distribution of arginine concentration of the flash frozen bottles but sampled differently. This shows that concentration of arginine is almost constant, at about 0.5–0.6 M. On the other hand, the arginine concentration of the liquid nitrogen frozen bottle that was allowed to thaw at 4 °C shows the similar gradient that has been described before (compare Fig. 9A with Fig. 6A) and the same is true for protein concentration gradient (not shown). These results demonstrate that the excipient gradient occurs mainly during thawing, although not exclusively. In order to examine the effect of the freezing process on gradient formation, an additional 2-L Teflon bottle containing 1.6 L of formulation buffer was frozen in a −80 °C freezer for 48 h and pieces of ice were sampled from different regions of the frozen bottle, then thawed at 4 °C and analyzed for arginine concentration. Fig. 9B shows the gradient of arginine in the ice of a bottle that was frozen under standard conditions at −80 °C with the data previously presented for the liquid nitrogen frozen bottle. The bottle frozen at −80 °C shows an increase in arginine concentration in those areas that are in the center (core) of the bottle. So it can be concluded that the gradients of the protein concentration and other components of the formulation buffer are formed primarily during thawing, not during freezing.

3.6. Biophysical characterization of thawed FGF-20 aliquots from 2-L bottles

Proteins undergo a variety of low temperature stresses during freeze-thawing (Chang et al., 1996; Wang, 2000; Arakawa et al., 2001) and these include: (i) cold denaturation, (ii) formation of ice that leads to a dramatic increase in concentration of all solutes, (iii) surface-induced denaturation at the ice–water interface, and (iv) pH change. All or some of these factors could lead to irreversible changes in the protein. In addition, during thawing, there could be a heterogeneous distribution in the concentration of solutes and pH (depending on thawing procedure). These may affect both solubility and stability of proteins. Therefore, it is important to characterize the protein at different regions of the container to evaluate whether the changes during the above-mentioned stresses are reversible or irreversible.

3.6.1. Assessment of tertiary structure by near-UV CD

Near-UV CD band originates from aromatic side chains that are immobilized in a folded protein structure, so it is sensitive to the natively folded structure of a protein. Therefore, near-UV CD spectra were used to determine if there were any differences in the tertiary structure of FGF-20 in various freeze–thaw samples. Near-UV CD spectra of various freeze–thaw samples (data not shown) were very similar to each other, suggesting that there is no change in tertiary structure of FGF-20 in the experimental condition.

3.6.2. Assessment of tertiary structure by steady-state fluorescence

Fluorescence is sensitive to the tertiary structure of a protein and depends on the local environment of fluorophores. In FGF-20, there are 1 tryptophan, 9 tyrosines and 10 phenylalanines. In the presence of tryptophan and tyrosine, contribution of phenylalanine to the observed fluorescence intensity is insignificant. Fluorescence is very sensitive to the local conformation around fluorophores and λ_{max} is sensitive to the polarity and solvent accessibility of fluorophores. Fluorescence spectra of different samples were recorded using excitation wavelengths of 283 and 295 nm. Excitation at 283 nm will result in fluorescence from both tryptophan and tyrosine residues, whereas excitation at 295 nm will result in fluorescence primarily from tryptophan. The contribution of tyrosines (even though small) was evident in the fluorescence spectra for the excitation wavelength of 283 nm in comparison to 295 nm excitation. However, there was no noticeable shift in λ_{max} in all the samples for a given excitation wavelength, indicating that solvent exposure of tryptophan remain unchanged. Fluorescence intensity of all the freeze–thaw samples were also similar (data not shown). So it can be concluded that that there is no irreversible change in tertiary structure of FGF-20 upon freeze–thawing.

3.6.3. Assessment of tertiary structure by second derivative near-UV absorption spectroscopy

Second derivative absorption spectroscopy has been used to resolve the complex spectrum in the near-UV region to evaluate quantitative contributions from phenylalanine, tryptophan and tyrosine residues (Balestrieri et al., 1978; Levine and Federici, 1982; Mach et al., 1995). This is because: (i) second derivative spectrum is highly resolved, (ii) second derivative function obeys the Beer–Lambert law, and (iii) peak absorption shifts blue upon unfolding of a protein.

Fig. 10 shows that spectra of all the freeze–thaw samples obtained from bottle-A were almost identical to each other as well

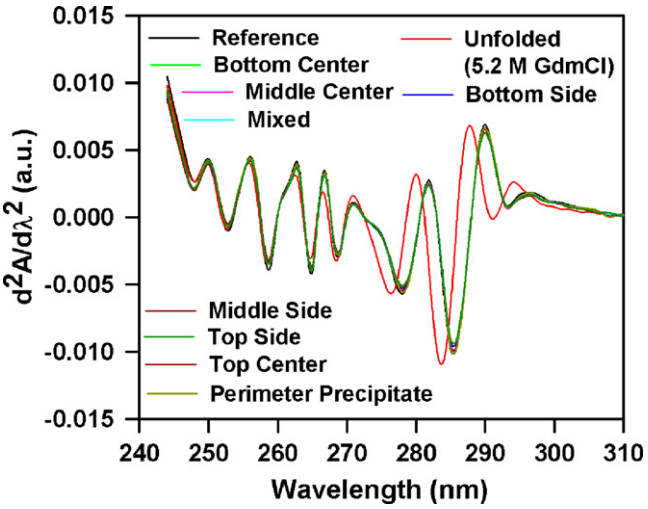

Fig. 10. Second derivative near-UV absorption spectra of various freeze–thaw samples collected from different regions of bottle-A. These spectra were recorded with a protein concentration of 0.39 mg/ml (monomer) in 50 mM phosphate, 0.1 M sodium sulfate, pH 7.0 at room temperature. For comparison, second derivative spectra of FGF-20 at a concentration of 0.39 mg/ml (monomer) were recorded for the reference sample and in the presence of 5.2 M GdmCl (unfolded protein) with the same buffer composition and experimental conditions.

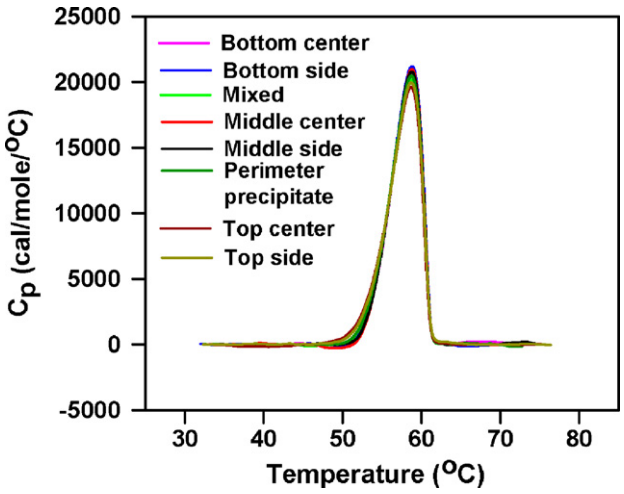

Fig. 11. DSC profiles of various freeze–thaw samples collected from different regions of bottle-A. These thermograms were recorded with a protein concentration of 1.0 mg/ml (monomer) in 50 mM phosphate (monobasic), 0.5 M arginine (sulfate), 0.01% Polysorbate 80, pH 7.0 with a scan rate of 30 °C/h.

as to the reference sample, which was not subjected to freeze–thaw. It also shows a blue shift of tyrosine and tryptophan absorption peaks of FGF-20 in the unfolded state. Similar results were obtained for all the freeze–thaw samples obtained from bottle-B (not shown). It is important to note that there was no difference in the second derivative spectra of various freeze–thaw samples obtained from bottles A and B. All these results suggest that freeze–thaw stresses did not make any noticeable irreversible conformational change in FGF-20 and the spectral characteristics of all the freeze–thaw samples in a given solution were similar to that of the reference sample. However, caution should be made in interpreting second derivative absorption spectra for evaluating conformational changes because these spectra are not very sensitive to the solvent polarity (Maity et al., in press).

3.6.4. Stability measured by differential scanning calorimetry (DSC)

Biochemical reactions involve changes in non-covalent interactions; therefore, associated heat effects are significantly lower than chemical reactions. DSC can be used to measure thermal stability of biomolecules. Generally, there is a direct correlation between thermal stability and formulation stability (aggregation and other deleterious effects) (Remmele et al., 1998; Remmele and Gombotz, 2000; Schön and Velazquez-Campoy, 2005; Wen et al., 2007; Guziewicz et al., 2007). Formulation stability increases with increase in thermal stability. A DSC experiment provides three typical parameters, ΔC_P, ΔH and T_m, where ΔC_P is the change in heat capacity between native and unfolded states, ΔH is the change in enthalpy at a given temperature and T_m is the mid-point of thermal denaturation.

Thermal unfolding of FGF-20 is irreversible due to aggregation, so equilibrium thermodynamics cannot be applied to obtain accurate thermodynamic parameters. When a thermal transition is associated with aggregation, the measured transition temperature (T_m) will be lower than that of a pure unfolding transition because unfolding is an endothermic process, whereas aggregation is exothermic. Due to these complexities, DSC thermal profiles were analyzed to obtain apparent mid-point of transition (T_m) and calorimetric enthalpy (ΔH_{cal}). In general, higher values for T_m and ΔH_{cal} are indicative of a higher stability. Native protein is enthalpically more stable than unfolded protein because packing and hydrogen bonding interactions contribute positively to the enthalpy.

Fig. 11 shows that normalized thermal profiles of different freeze–thaw samples obtained from bottle-A are very similar to one another. The corresponding values of T_m and ΔH_{cal} are given in Table 4. These results suggest that there were no changes in the thermodynamic stabilities of various freeze–thaw samples of FGF-20 at different parts of the bottle under the experimental conditions. Similar results were also obtained for samples taken from bottle-B (Table 4). A DSC thermogram was recorded for a freshly purified batch of FGF-20 as a reference. Table 4 shows no significant change in T_m and ΔH_{cal} between freeze–thaw samples and the reference. Small differences in T_m and ΔH_{cal} may be due to the fact that the freeze–thaw samples and the control were from two different batches. These results demonstrate that there is no change in thermodynamic stability of FGF-20 upon freeze–thawing.

3.6.5. Measurement of stability by denaturant induced unfolding

Denaturant induced unfolding is a powerful method to measure thermodynamic stability of proteins. The majority of denaturant induced unfolding reactions are reversible, so using equilibrium thermodynamic analysis, ΔG, m, and C_m are obtained. ΔG is the unfolding free energy, m-value is related to the change in accessible

Table 4
Thermal stability parameters determined from DSC profiles of freeze–thaw samples obtained at different regions of the 2-L bottles (A and B).

Sample ID	Bottle ID	T_m (°C)	ΔH_{cal} (kcal/mol)
Bottom center (BC)	A	58.8	100.2
Bottom center (BC)	B	58.6	97.0
Bottom side (BS)	A	58.8	101.3
Bottom side (BS)	B	58.6	98.0
Middle center (MC)	A	58.8	98.7
Middle center (MC	B	58.7	98.8
Middle side (MS)	A	58.7	99.1
Middle side (MS	B	58.7	97.3
Perimeter precipitate (PP)	A	58.8	99.9
Perimeter precipitate (PP)	B	58.7	98.2
Mixed (M)	A	58.8	99.4
Mixed (M)	B	58.7	99.7
Top side (TS)	A	58.7	100.8
Top side (TS)	B	58.7	97.3
Top center (TC)	A	58.7	99.9
Top center (TC)	B	58.7	96.9
Reference	N.A.	59.0	102.0

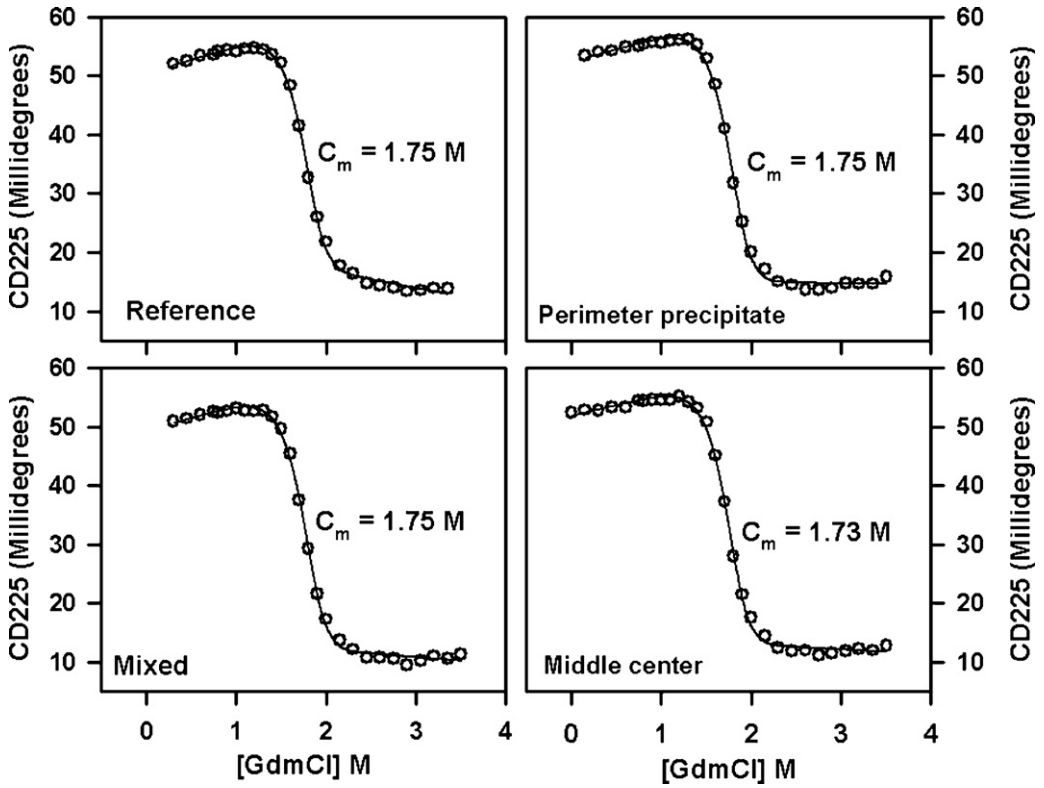

Fig. 12. GdmCl induced unfolding of Mixed, perimeter precipitate and middle center freeze–thaw samples (bottle-A) along with reference sample. Experiments were performed in 0.1 M potassium phosphate (dibasic), 0.2 M KCl, 9.9 mM arginine (sulfate) pH 7.0 with a protein concentration of 8.78 μM (monomer). Titration was done by 5.42 M GdmCl solution containing 0.1 M potassium phosphate (dibasic), 0.2 M KCl pH 7.0. Unfolding transition was monitored by far-UV CD at 225 nm at 20 °C.

surface area upon unfolding and C_m is the mid-point of transition. These parameters are very useful to understand stability of proteins. Both CD and fluorescence can be used to monitor denaturant induced unfolding transitions.

Fig. 12 shows the GdmCl induced unfolding of various freeze–thaw and reference samples of FGF-20 monitored by far-UV CD. All these transitions are apparently monophasic and as FGF-20 is a dimeric protein, and for simplicity, data was analyzed by a two-state dimeric unfolding model involving native dimer and unfolded monomeric forms (Maity et al., 2005, in press). This model fits very well with all the data sets, and the parameters obtained from the analysis are shown in Table 5. It is important to note that the *m*-value (which is proportional to the change in accessible surface area upon unfolding) is model dependent and the presence of an intermediate can alter the value to a different extent depending on the amount of population (Mayne and Englander, 2000; Maity et al., 2003, 2004, 2006; Eftink and Ionescu, 1997). On the other hand, mid-point of transition could be measured quite accurately. However, as we are comparing stabilities under the same experimental condition, it is appropriate to compare all parameters. Here, we have measured stability of three different freeze–thaw samples from bottle-A: middle center, perimeter precipitate, mixed, and a reference. It is important to note that middle center and perimeter precipitate samples were cloudy, whereas the mixed sample was clear. So stability measurements of these samples are expected to give the overall picture of the stability of all freeze–thaw samples.

Table 5
Parameters for GdmCl induced unfolding of freeze–thaw samples of FGF-20 (bottle-A) and reference sample.

Sample ID	C_m (M)	*m* (kcal/mol M)	$\Delta G_{0,un}$ (kcal/mol)
Reference	1.75	7.0	19.1
Mixed	1.75	6.8	18.6
Middle center	1.74	6.7	18.5
Perimeter precipitate	1.75	6.8	18.7

Unfolding free energy ($\Delta G_{0,un}$) of FGF-20 is about 18.5 kcal/mol, suggesting that it is a stable protein. Table 5 shows that all the parameters of various samples were very similar, indicating there is no detectable change in the stability of all these samples. The fluorescence transitions of GdmCl induced unfolding of various freeze–thaw samples along with the reference, are multi-phasic and hence were not used for analysis. However, qualitatively, all these transitions were similar, indicating that there was no noticeable change in stability among various samples. Here again, these results demonstrate there was no detectable change in thermodynamic stability of FGF-20 upon freeze–thawing.

3.6.6. *Isoform distributions monitored by RP-HPLC*

RP-HPLC is one of the most commonly used chromatographic techniques for analysis of biomolecules. The resolution power of a properly developed RP-HPLC method is so efficient that it can separate polypeptides that differ by a single amino acid. Separation of biomolecules on a RP-HPLC column is based on subtle differences in the "hydrophobic foot." Protein degradation products due to deamidation and oxidation can be evaluated by RP-HPLC. The reverse phase chromatograms of some freeze–thaw samples (not shown) that had significant concentration gradients in protein and solutes upon freeze–thaw are very similar to each other, suggesting that there was no considerable difference in the isoform distribution among various samples.

4. Conclusions

All the characterization data presented here indicates that FGF-20 sampled from different regions of the thawed bottle is similar in

stability, structural characteristics and isoform distribution. Thus, the concentration gradient generated after thawing does not cause any irreversible change in conformation or stability of FGF-20. These concentration gradients resulted in an appearance of turbidity in the top and bottom layers during thawing. However, this turbidity is due to a lower solubility of FGF-20 in those conditions and not due to any irreversible changes of the protein.

The FGF-20 drug substance can be thawed without irreversible precipitation by three methods and these are: (a) thawing at 4 °C with gentle shaking (about 100 rpm in a standard shaker), (b) thawing at room temperature with gentle shaking, and (c) thawing at 4 °C standing. The first two methods produce no precipitate whereas the third method may produce precipitate that readily goes back into solution upon mixing. The pH of the frozen solution and the concentration of Polysorbate 80 in the formulation were found not to be relevant to the precipitation of FGF-20. The breakthrough in the understanding of the cause of FGF-20 precipitation came from the measurements of arginine, sulfate and phosphate in different parts of the thawed bottle. It was found that a gradient is formed primarily upon thawing, and that the concentration of arginine and sulfate at the top of the melted solution was not enough to maintain the protein in solution. On the other hand, the excipient concentration at the bottom of the bottle was high enough to induce the precipitation of the protein in some cases by a *salting out* effect. Freezing bottles in liquid nitrogen produces a homogenous solid in terms of arginine concentration. When these bottles are thawed, the profiles of the arginine and protein concentrations are similar to the bottles frozen in a −80 °C freezer, indicating that the excipient and protein gradient is mainly formed during thawing.

Acknowledgements

We thank Anitha Palamakula, Daniel Wagner, Ethan DeFord and Chelsea Mays for their assistance in performing some of these experiments.

Appendix A. Heat transfer during freeze–thawing

There are three basic modes of heat transfer and these are: (i) conduction, (ii) convection, and (iii) radiation. According to Fourier's law, the rate of heat transfer in the conduction mode is directly proportional to the temperature gradient and inversely proportional to the thickness of the wall, and can be written as (Nag, 1989)

$$Q = -K \times A\frac{T_2 - T_1}{x} \tag{A.1}$$

where K is the thermal conductivity of the material through which heat is being transferred, A is the surface area of the container, $(T_2 - T_1)$ is the temperature difference across the wall and x is the thickness of the wall. For a cylindrical container the rate of heat transfer due to conduction can be written as (Nag, 1989)

$$Q = \frac{K(A_2 - A_1)(T_1 - T_2)}{(r_2 - r_1)\ln A_2/A_1} \tag{A.2}$$

where A_1 and A_2 are the inside and outside surface areas, and r_1 and r_2 are the internal and external radius of the cylinder, respectively.

Heat transfer due to convection involves movement of fluids that could occur as a result of difference in solution density in the present experimental model. Here, the convection process of heat transfer is free, or natural, as there was no external device used for the fluid motion. Let us consider the temperature of a very thin layer of fluid adjacent to the container wall varies from T_w to T_f due to a free or natural convection process. According to Newton's law of cooling, one can write the rate of heat transfer (Q) similar to Eq. (A.1) as

$$Q = -K_f A\frac{T_f - T_w}{x} = hA(T_W - T_f) \tag{A.3}$$

where K_f is the thermal conductivity of the adjacent thin layer of the fluid and $h = K_f/x$ is the coefficient of heat transfer. During heat transfer from the liquid to the cold atmosphere in the −80 °C freezer through the bottle wall, one can think of three resistances in series and can be expressed as $R = R_f + R_w + R_{CA}$. R_f, R_w and R_{CA} are the resistance for the heat transfer in the fluid, wall and cold atmosphere, respectively. One can write the total rate of heat transfer as

$$Q = \frac{T_f - T_{CA}}{R} \tag{A.4}$$

T_f and T_{CA} are the temperature of the fluid and cold atmosphere in the freezer, respectively. In addition to conduction and convection, heat will also be transferred by radiation.

Appendix B. Supplementary data

Supplementary data associated with this article can be found, in the online version, at doi:10.1016/j.ijpharm.2009.05.063.

References

Alvarez, E., Fey, E.G., Valax, P., Yim, Z., Peterson, J.D., Mesri, M., Jeffers, M., Dindinger, M., Twomlow, N., Ghatpande, A., LaRochelle, W.J., Sonis, S.T., Lichenstein, H.S., 2003. Preclinical characterization of CG53135 (FGF-20) in radiation and concomitant chemotherapy/radiation-induced oral mucositis. Clin. Cancer Res. 9, 3454–3461.

Anchordoquy, T.J., Carpenter, J.F., 1996. Polymers protect lactate dehydrogenase during freeze-drying by inhibiting dissociation in the frozen state. Arch. Biochem. Biophys. 332, 231–238.

Arakawa, T., Prestrelski, S.J., Kenney, W.C., Carpenter, J.F., 2001. Factors affecting short-term and long-term stabilities of proteins. Adv. Drug Deliv. Rev. 46, 307–326.

Balestrieri, C., Colonna, G., Giovane, A., Irace, G., Servillo, L., 1978. Second-derivative spectroscopy of proteins. Eur. J. Biochem. 90, 433–440.

Chang, B.S., Kendrick, B.S., Carpenter, J.F., 1996. Surface-induced denaturation of proteins during freezing and its inhibition by surfactants. J. Pharm. Sci. 85, 1325–1330.

Eftink, M.R., 1994. The use of fluorescence methods to monitor unfolding transitions in proteins. Biophys. J. 66, 482–501.

Eftink, M.R., Ionescu, R., 1997. Thermodynamics of protein unfolding: questions pertinent to testing the validity of the two-state model. Biophys. Chem. 64, 175–197.

Eftink, M.R., Maity, H., 2000. Spectroscopy and spectrofluorimetry. A practical approach. In: Gore, M.G. (Ed.), Use of Optical Spectroscopic Methods to Study the Thermodynamic Stability of Proteins. IRL Press, Oxford, pp. 307–327.

Fan, H., Vitharana, S.N., Chen, T., O'Keefe, D., Middaugh, C.R., 2007. Effects of pH and polyanions on the thermal stability of fibroblast growth factor 20. Mol. Pharm. 4, 232–240.

Gómez, G., Pikal, M.J., 2001. Effect of initial buffer composition on pH changes during far-from equilibrium freezing of sodium phosphate buffer solutions. Pharm. Res. 18, 90–97.

Guziewicz, N., Trierweiler, G., Johnson, K., Simler, R., Perez-Ramirez, B., 2007. Probing the solution behavior of proteins by differential scanning calorimetry: applications to pre-formulation and formulation development. In: Reese, E.L., Spotts, S. (Eds.), Proceedings of the 2007 Current Trends in Microcalorimetry Conference. MicroCal LLC, Northampton, pp. 127–153.

Jeffers, M., Shimkets, R., Prayaga, S., Boldog, F., Yang, M., Burgess, C., Fernandes, E., Rittman, B., Shimkets, J., LaRochelle, W.J., Lichenstein, H.S., 2001. Identification of a novel human fibroblast growth factor and characterization of its role in oncogenesis. Cancer Res. 61, 3131–3138.

Jeffers, M., McDonald, W.F., Chillakuru, R.A., Yang, M., Nakase, H., Deegler, L.L., Sylander, E.D., Rittman, B., Bendele, A., Sartor, R.B., Lichenstein, H.S., 2002. A novel human fibroblast growth factor treats experimental intestinal inflammation. Gastroenterology 123, 1151–1162.

Kirikoshi, H., Sagara, N., Saitoh, T., Tanaka, K., Sekihara, H., Shiokawa, K., Katoh, M., 2000. Molecular cloning and characterization of human FGF-20 on chromosome 8p21.3–p22. Biochem. Biophys. Res. Commun. 274, 337–343.

Levine, R.L., Federici, M.M., 1982. Quantitation of aromatic residues in proteins: model compounds for second-derivative spectroscopy. Biochemistry 21, 2600–2606.

Mach, H., Volkin, D.B., Burke, C.J., Middaugh, C.R., 1995. Ultraviolet absorption spectroscopy. Methods Mol. Biol. 40, 91–114.

Maity, H., Lim, W.K., Rumbley, J.N., Englander, S.W., 2003. Protein hydrogen exchange mechanism: local fluctuations. Protein Sci. 12, 153–160.

Maity, H., Maity, M., Englander, S.W., 2004. How cytochrome *c* folds, and why: submolecular foldon units and their stepwise sequential stabilization. J. Mol. Biol. 343, 223–233.

Maity, H., Rumbley, J.N., Englander, S.W., 2006. Functional role of a protein foldon-An Ω-loop foldon controls the alkaline transition in ferricytochrome *c*. Proteins 63, 349–355.

Maity, H., Mossing, M.C., Eftink, M.R., 2005. Equilibrium unfolding of dimeric and engineered monomeric forms of λ Cro (F58W) repressor and the effect of added salts: evidence for the formation of folded monomer induced by sodium perchlorate. Arch. Biochem. Biophys. 434, 93–107.

Maity, H., Karkaria, C., Davagnino, J., in press. Effects of pH and arginine on the solubility and stability of a therapeutic protein (Fibroblast Growth Factor 20): relationship between solubility and stability. Curr. Pharm. Biotechnol. 10.

Mayne, L., Englander, S.W., 2000. Two-state vs. multistate protein unfolding studied by optical melting and hydrogen exchange. Protein Sci. 9, 1873–1877.

Myers, J.K., Pace, C.N., Scholtz, J.M., 1995. Denaturant *m* values and heat capacity changes: relation to changes in accessible surface areas of protein unfolding. Protein Sci. 4, 2138–2148.

Nag, P.K., 1989. Engineering Thermodynamics. Tata McGraw-Hill Publishing Company Ltd, New Delhi, India.

Nozaki, Y., 1972. The preparation of guanidinium chloride. Methods Enzymol. 26, 43–50.

Pace, C.N., 1986. Determination and analysis of urea and guanidine hydrochloride denaturation curves. Methods Enzymol. 131, 266–280.

Pikal-Cleland, K.A., Cleland, J.L., Anchordoquy, T.J., Carpenter, J.F., 2002. Effect of glycine on pH changes and protein stability during freeze–thawing in phosphate buffer systems. J. Pharm. Sci. 91, 1969–1979.

Plotnikov, A.N., Eliseenkova, A.V., Ibrahimi, O.A., Shriver, Z., Sasisekharan, R., Lemmon, M.A., Mohammadi, M., 2001. Crystal structure of fibroblast growth factor 9 reveals regions implicated in dimerization and autoinhibition. J. Biol. Chem. 276, 4322–4329.

Remmele, R.L., Nightlinger, N.S., Srinivasan, S., Gombotz, W.R., 1998. Interleukin-1 receptor (IL-1R) liquid formulation development using differential scanning calorimetry. Pharm. Res. 15, 200–208.

Remmele, R.L., Gombotz, W.R., 2000. Differential scanning calorimetry: a practical tool for elucidating stability of liquid pharmaceuticals. Biopharm. Eur. 56, 58–60.

Schön, A., Velazquez-Campoy, A., 2005. In: Jiskoot, W., Crommelin, D. (Eds.), Methods for Structural Analysis of Protein Pharmaceuticals. AAPS Press, Arlington, pp. 573–589.

van der Walt, J.M., Noureddine, M.A., Kittappa, R., Hauser, M.A., Scott, W.K., McKay, R., Zhang, F., Stajich, J.M., Fujiwara, K., Scott, B.L., Pericak-Vance, M.A., Vance, J.M., Martin, E.R., 2004. Fibroblast growth factor 20 polymorphisms and haplotypes strongly influence risk of Parkinson disease. Am. J. Hum. Genet. 74, 1121–1127.

Wang, G., van der Walt, J.M., Mayhew, G., Li, Y.J., Züchner, S., Scott, W.K., Martin, E.R., Vance, J.M., 2008. Variation in the miRNA-433 binding site of FGF20 confers risk for Parkinson disease by overexpression of alpha-synuclein. Am. J. Hum. Genet. 82, 283–289.

Wang, W., 2000. Lyophilization and development of solid protein pharmaceuticals. Int. J. Pharm. 203, 1–60.

Wen, J., Jiang, Y., Narhi, L., Hymes, K., Gong, K., 2007. Correlation between thermal stability and protein stability. In: Reese, E.L., Spotts, S. (Eds.), Proceedings of the 2007 Current Trends in Microcalorimetry Conference. MicroCal LLC, Northampton, pp. 93–108.